Accepted Manuscript

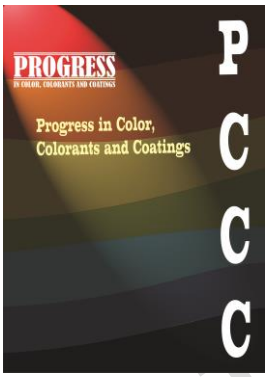

Title: Hybrid DOE–RSM modeling of antibacterial and mechanical performance of ZnO–CMC paper coatings

Authors: Sousan Rasouli, Faegheh sadat Mortazavi Moghadam, Majid Ghoreishi

Manuscript number**: PCCC-2601-1491**

To appear in: Progresss in Color, Colorants and Coatings

Received: 13 January 2026

Final Revised: 23 May 2026

Accepted: 29 May 2026

Please cite this article as:

S. Rasouli, F. S. Mortazavi Moghadam, M. Ghoreishi, Hybrid DOE–RSM modeling of antibacterial and mechanical performance of ZnO–CMC paper coatings, Prog. Color, Colorants, Coat., 20 (2027) XX-XXX.

DOI: 10.30509/pccc.2026.167760.1491

Hybrid DOE–RSM Modeling of Antibacterial and Mechanical Performance of ZnO–CMC Paper Coatings

S. Rasouli [*a] , F. S. Mortazavi Moghadam [**b], M. Ghoreishi[b]

a Department of Nanomaterials & Nanocoatings, Institute for Color Science and Technology (ICST), P.O. Box: 16765-654, Tehran, Iran

b Department of Mechanical Engineering, K. N. Toosi University of Technology, P.O. Box: 16315-1355, Tehran, Iran

Corresponding author's email address: * rasouli@icrc.ac.ir; ** mortazavi_faeghe@yahoo.com

Abstract

In this study, zinc oxide (ZnO) nanoparticles were synthesized using the glycine-nitrate combustion method and structurally and morphologically characterized. X-ray diffraction (XRD) results confirmed the formation of pure ZnO phase with wurtzite structure and nano-crystalline nature of particles, average crystallite size was calculated at 37 nm. Electron microscopy SEM-TEM images confirmed the quasi-spherical morphology of nanoparticles. In order to evaluate the bio-efficacy of the synthesized nanoparticles, minimum inhibitory concentration (MIC) and minimum bactericidal concentration (MBC) tests of the synthesized ZnO nanoparticles against *Staphylococcus aureus* and *Escherichia coli* bacteria were performed and biologically effective concentration range was selected for use in coating suspension. ZnO nanoparticles were added to carboxymethylcellulose (CMC) base coatings at selected concentrations and applied to paper. Using a full factorial design of experiments (DOE), the simultaneous effect of

ZnO concentration and coating thickness on the antibacterial index (R), tensile strength, and burst strength of the coated paper was investigated. Statistical analysis and response surface methodology (RSM) were used to model the main and interaction effects of parameters and develop predictive models. The results showed that ZnO concentration and coating thickness play a decisive role in the antibacterial performance and mechanical properties. Multi-response optimization was performed considering the maximization of antibacterial property and mechanical properties of the paper. The proposed DOE–RSM hybrid framework provides an effective and reliable approach for the design and optimization of antibacterial paper coatings, what the optimize results are related to ZnO (wt%); 7.55%, and Thickness (μm)120**.**

Keywords: Carboxymethylcellulose, Antibacterial paper coating, Design of experiments (DOE), Utility function optimization, Mechanical properties.

1. Introduction

Humans have long faced the problem of food preservation because of many microorganisms in the environment [1]. Using the food source, they multiply after a while the food becomes spoiled and unusable [2]. In this context, bacteria are of particular importance. Bacteria have the ability to grow and create biofilms on various surfaces that cause spoilage in food [3]. In this study, two strains of Gram-negative and Gram-positive bacteria, *Escherichia coli* and *Staphylococcus aureus*, were selected as model microorganisms due to their widespread presence in food systems and their importance as indicators of health quality. *Escherichia coli* widely causes food- and

waterborne poisoning and diseases [4], while *Staphylococcus aureus* has high resistance to environmental stresses with the ability to produce toxins [5]. Therefore, simultaneous examination of these two bacterial strains can provide a proper assessment of antibacterial performance against Gram-negative and Gram-positive microorganisms . Also, in order to address concerns about bacterial spoilage, the development of antibacterial materials has received widespread attention, especially in the packaging, hygiene, and paper industries. While the hydrophilic nature and porous structure of paper provide a medium for the growth and transmission of microorganisms [6, 7], it is considered an important option for the production of functional materials due to its biodegradability, accessibility, and wide application. Therefore, the use of antibacterial materials in the surface coating of paper could be an important issue in increasing its safety and efficiency [7].

Zinc oxide, suitable option as an inorganic antibacterial agent, has good chemical stability and high environmental compatibility [8]. The antibacterial properties of ZnO can be explained by the production of reactive oxygen species, direct interaction with the bacterial cell wall, and the release of Zn^{2+} ions [9]. At the nanometer scale, the antibacterial properties of zinc dioxide particles are improved significantly with increasing particle surface area [10]. As a result, controlling the synthesis method can play an important role in the final efficiency of their properties [11]. On the other hand, biopolymers such as carboxymethylcellulose (CMC) can be considered as a good matrix for the application of antibacterial agents such as zinc oxide. Biodegradability, proper adhesion to paper fibers and film-forming ability are important characteristics of carboxymethylcellulose in its application in paper coating formulations.

Although the combination of CMC with ZnO nanoparticles can provide antibacterial properties and improve the mechanical properties of paper, improper selection of concentration or processing conditions can cause a decrease in mechanical properties. Therefore, simultaneous optimization of antibacterial performance and mechanical properties is essential [12, 13]. In many previous studies, the selection of ZnO concentration in coatings has been done experimentally and without specific biological support [14, 15]. While excessive use of nanoparticles disrupts the proper balance between antibacterial performance and mechanical properties of the coating [12]. In this regard, the use of minimum inhibitory concentration (MIC) and minimum bactericidal concentration (MBC) tests can provide a suitable scientific basis for determining the biologically effective concentration range of nanoparticles [4, 16]. To avoid the classic and inefficient trial-and-error method in multi-factor systems, the use of Design of Experiments (DOE) and especially Response Surface Methodology (RSM) are considered as powerful statistical tools for simultaneously examining the effects of various factors and their interactions with a minimum number of experiments.

The aim of this study is to provide optimal conditions for the preparation of ZnO–CMC for paper coating, to be within the range of effective biological concentrations to ensure antibacterial effectiveness, prevent excessive consumption of nanoparticles and establish a proper balance between antibacterial performance and maintaining or improving the mechanical properties of the paper. In this regard, ZnO nanoparticles are synthesized by glycine–nitrate combustion method and their antibacterial performance in CMC-based coatings on paper is evaluated using MIC and MBC tests. The simultaneous effect of ZnO concentration and coating thickness on antibacterial index (R) and mechanical

properties including tensile and burst strength are investigated using DOE and system modeling and optimization are performed using RSM approach. This study provides a systematic and reliable framework for the design and optimization of antibacterial paper coatings that may support future industrial development. This study provides a systematic and reliable framework for the design and optimization of antibacterial paper coatings that can support future industrial development. The present study focuses on laboratory-scale performance evaluation within a defined experimental design space and does not aim to address regulatory validation, long-term durability, or migration assessment.

2. Experimental

2.1. Materials

Zinc nitrate hexahydrate ($Zn(NO_3)_2 \cdot 6H_2O$) and glycine ($C_2H_5NO_2$), carboxymethylcellulose (CMC), with a very high purity (99.9%) were purchased from Sigma-Aldrich, and deionized water was used in all steps. Carboxymethylcellulose was used as the bio-matrix of the coating. All solutions were prepared using distilled water.

2.2. Synthesis of ZnO nanoparticles

Zinc oxide (ZnO) nanoparticles were synthesized using the glycine-nitrate combustion method [17]. In this method, 2.5 g of zinc nitrate hexahydrate was dissolved in 2 mL of deionized water. 0.84 g of glycine was dissolved in 2 mL of distilled water separately. Then, the two solutions were mixed together and subjected to stirring while heating on a hotplate until gelation occurred. To complete the combustion reaction, the resulting gel was transferred to a porcelain crucible and subjected to heat treatment at 350 °C for 30

min. After cooling, the obtained product was washed with distilled water and ethanol and dried at 100 °C for 12 h.

The synthesis of zinc oxide nanoparticles was carried out using the glycine-nitrate combustion method based on an exothermic redox reaction, the general equation of which is expressed as equation 1:

$$9Zn(NO_3)_2.6H_2O+10NH_2CH_2COOH \rightarrow 9ZnO+20CO_2+79H_2O+14N_2 \quad (1)$$

During the heating process, the precursor solution containing zinc nitrate and glycine turn into a viscous liquid and then spontaneously ignites is occurred. This rapid combustion leads to the formation of a porous, foamy, and voluminous mass, a characteristic feature of combustion methods. The heat released in this process is due to the redox reaction between nitrate ions as the oxidizing agent and glycine as the reducing agent. This process provides the necessary conditions for rapid formation of the oxide phase and prevents excessive grain growth. A schematic view of the synthesis steps of ZnO nanoparticles is presented in Figure 1.

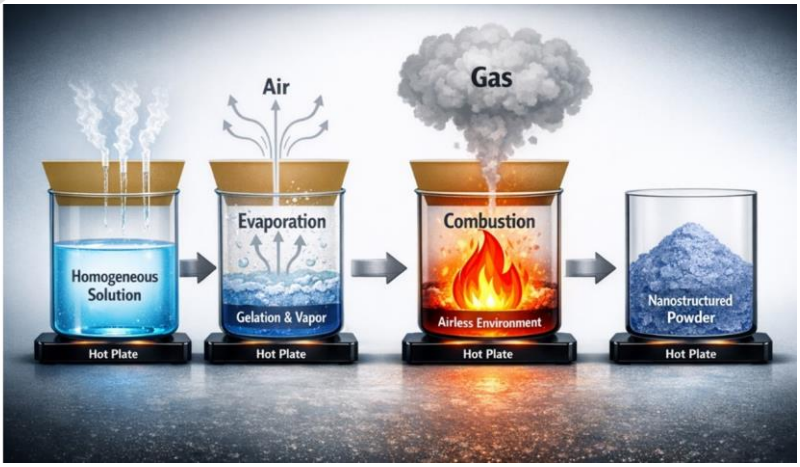

Figure 1 - Schematic view of the synthesis of nano zinc oxide.

From an environmental perspective, the glycine–nitrate combustion method used for ZnO synthesis can be considered a relatively eco-friendly approach with a low pollution footprint. The synthesis employs water as a green solvent and glycine, a non-toxic amino acid, as the fuel and complexing agent. Moreover, the highly exothermic redox reaction enables the rapid formation of the ZnO phase at a relatively low external temperature (350 °C) and short reaction time, thereby reducing overall energy consumption. According to the reaction stoichiometry (Equation 1), the gaseous by-products generated during the combustion process mainly consist of H_2O, CO_2, and N_2. Furthermore, incorporating these nanoparticles into a biodegradable cellulosic paper substrate provides a sustainable alternative to conventional plastic materials and may help reduce waste through improved antibacterial performance.

2.3. Structural and morphological studies of ZnO nanoparticles

The crystal structure of the synthesized nanoparticles was investigated using X-ray diffraction (XRD). The crystalline phase was identified by comparing the diffraction patterns with reference data and the average crystallite size was calculated using the Debye-Scherer relationship 2.

$$D = \frac{K\lambda}{\beta \cos \theta} \quad (2)$$

D is the average crystallite size, λ is the X-ray wavelength, β is the half-maximum width of the diffraction peak, and θ is the Bragg angle.

The morphology and size of the particles were investigated using scanning electron microscopy (SEM) and transmission electron microscopy (TEM)

2.4. Preparation of ZnO nanoparticle suspension, MIC and MBC tests

2.4.1. MIC test

The minimum inhibitory concentration (MIC) of ZnO nanoparticles was determined according to the method reported by Mortazavi Moghadam et al. [16]. Suspensions of ZnO nanoparticles with concentrations of 0.1, 0.5, 1, 1.5 and 2 mg/mL were prepared by dispersing the nanoparticles in deionized water. To perform the MIC test, 1 mL of nutrient broth (NB) culture medium was added to sterile tubes. Then, 50 µL of bacterial suspension adjusted according to 0.5 McFarland standard (approximately 1.5×10^8CFU/mL) of *Escherichia coli* (PTCC 1399) and *Staphylococcus aureus* (PTCC 1431) bacteria was added to each tube. After addition of the nanoparticle suspension, the samples were incubated for 24 hours at 37°C. The lowest concentration that prevented visible bacterial growth was recorded as the MIC value. The uniformity of bacterial inoculation was confirmed by measuring the optical density at a wavelength of 600 nm. All MIC experiments were conducted in triplicate to ensure the reliability and reproducibility of the results.

2.4.2. MBC test

The minimum bactericidal concentration (MBC) was determined using the broth microdilution method, following the same experimental framework as reported by Mortazavi Moghadam et al. [16]. For this purpose, tubes containing 2 mL of nutrient broth culture medium and concentrations of 0.5, 1, 1.5 and 2 mg/mL of ZnO nanoparticles were prepared. Then, 25 µL of bacterial suspension was added to each tube and the samples were incubated for 24 hours at 37 °C. The lowest concentration that

resulted in no bacterial growth was determined as the MBC value. The results of the MIC and MBC tests were used as the basis for selecting the concentration levels of ZnO nanoparticles for the formulation of the coating suspension. All MBC measurements were conducted in triplicate to ensure reproducibility of the results.

2.5. Preparation of CMC–ZnO coating suspension

The coating base solution was prepared by preparing an aqueous solution of 1% weight-volume (wt. %) carboxymethylcellulose. Then, ZnO nanoparticles were added to the CMC solution at four concentration levels of 1.5, 3, 6, and 9% weight (wt. %). In order to achieve uniform distribution of nanoparticles, the suspensions were homogenized using an Ultra-Turrax homogenizer (IKA T25 Digital, Germany) at a speed of 10,000 rpm for 3 minutes.

2.6. Preparation of papers

2.6.1. Handmade base-paper

In this study, in order to control the parameters and reduce the incidence of errors, the papers used were made according to the T 205 SP-02 standard, for which ILIM CO, Russia, high-brightness (TAPPI T 452 om-98 standard :87%) bleached kraft softwood pulp and a handmade paper machine (P41521.159, Austria) were used. Then, their preparation for the coating process was carried out according to the T 402 om-98 standard.

2.6.2. Paper coating and drying process

The paper was coated using an automatic rod coating machine (Dongguan Lonroy Equipment, China). The coating thickness was set at four levels of 30, 60, 90, and 120 μm using calibrated bar applicators with predefined gap settings corresponding to nominal wet film thicknesses. After coating, the samples were dried using a laboratory UV–IR dryer (BE 20, Systec, Germany) at a controlled temperature of 60 °C for 10 minutes under moderate IR intensity. The controlled drying conditions were selected to ensure gradual solvent evaporation and to prevent rapid surface skin formation, which could negatively affect coating integrity. All samples were dried under identical conditions to ensure reproducibility and comparability of mechanical and antibacterial results. Following drying, the actual coating thickness was measured using a PT-200-S3 Advanced thickness gauge (PCE, USA). Thickness measurements were performed at multiple randomly selected positions on each sample. The low variation among measured points confirmed acceptable coating thickness uniformity.

2.6.3. Conditioning of samples

Prior to mechanical testing, all paper samples (both uncoated and coated) were conditioned according to TAPPI T 402 om-98 standard at 23 ± 1 °C and 50 ± 2% relative humidity for at least 24 hours. This conditioning ensured moisture equilibrium and minimized environmental effects on tensile and burst strength measurements.

2.7. Evaluation of antibacterial performance of coatings

The antibacterial performance of the coated papers was evaluated quantitatively according to the Japanese Industrial Standard (JIS Z 2801) protocol, with minor

modifications adapted from Mortazavi Moghadam et al. [16]. The samples were cut into 10×10 mm pieces. Standard suspensions of bacteria (*S. aureus* and *E. coli*) were prepared and adjusted to a turbidity of 0.5 McFarland standard (approximately 1.5×10^8 CFU/ML). The bacterial suspensions were directly inoculated onto the surface of the composite samples and covered with a sterile polyethylene film to ensure uniform contact. The inoculated samples were incubated at 37 °C under high relative humidity (≥ 90%) for 24 h (contact time). After the contact period, the surviving bacteria were recovered and subjected to 10-fold serial dilutions. From each dilution, the bacteria were plated on agar and incubated for 48 h at 37 °C. After incubation, the visible bacterial colonies were counted and expressed as Colony Forming Units (CFU/cm^2). Finally, the antibacterial activity number (R) was calculated according to the following equation 3:

$$R = \log\left(\frac{B}{A}\right) \quad (3)$$

where B is the number of colonies in the control sample and A is the number of colonies in the coated sample. Each antibacterial assay was performed in ten independent replicates (n = 10), and the results were reported as mean ± standard deviation.

2.8. Mechanical tests of paper

The tensile properties of the samples were measured using a universal testing machine (GOTECH AI-300) according to the TAPPI T 494 om-01 standard (constant rate of elongation method). For each treatment level, 30 independent specimens were tested (n = 30) to ensure statistical reliability. Results were reported as mean ± standard deviation. Bursting strength was determined using a DRK 109 device based on the TAPPI T 403

om-97 standard. A total of 20 specimens per condition (n = 20) were evaluated for burst strength, and the results were expressed as mean ± standard deviation.

2.9. Brightness of paper

The brightness value of the paper samples was measured according to the TAPPI T 452 om-98 standard with five replicates. Results were reported as mean ± standard deviation. Since brightness was not included as a response variable in the factorial experimental design, it was analyzed descriptively and was not incorporated into the RSM optimization model.

2.10. Design of Experiments (DOE) and RSM Modeling

2.10.1. Design of Experiments (DOE) and Data Structure

In order to systematically investigate the effects of process parameters on the antibacterial and mechanical performance of coated paper, the experiments were designed using a full factorial (4×4) design consisting of two factors at four levels each. The factors s included the concentration of ZnO nanoparticles in the coating (1.5, 3, 6 and 9 wt.%) and the thickness of the coating (30, 60, 90 and 120 μm), resulting in 16 experimental combinations. Each combination was performed in independent replicates and the results were reported as mean and standard deviation. The responses evaluated included the antibacterial index (R), tensile strength and burst strength of the paper. The selection of ZnO nanoparticles concentration levels was based on the results of MIC and MBC tests. It should be noted that the present study employed a two-factor full factorial design (4×4) rather than a Box–Behnken design (BBD). Therefore, higher-order cubic

modeling was not considered necessary for the investigated system.

2.10.2. Statistical analysis and DOE-based modeling

To evaluate the effects of process factors and their interactions on the responses under study, the experimental data were first analyzed using two-way ANOVA. In this analysis, the main effect of ZnO nanoparticles concentration in the coating, the main effect of coating thickness, and the interaction effect of these two factors on each of the responses were examined independently. The statistical significance of the effects was assessed based on the probability value (p-value) at the 95% confidence level ($\alpha = 0.05$). In addition to reporting p-values, to more accurately interpret the results and avoid misleading perceptions in situations where the range of response changes is limited, effect size indices such as partial eta square and omega square were also used.

2.10.3. Response Surface Modeling (RSM)

After the initial statistical analysis, the Response Surface Methodology was used to develop predictive models and enable process optimization. To describe the relationship between the independent variables and the responses and based on the two-factor nature of the system a second-order quadratic polynomial model was considered. Given the two-factor nature of the system and the absence of higher-order interaction terms, a quadratic polynomial model was sufficient to describe the response behavior within the studied design space. In this model, the responses included antibacterial index, tensile strength, and burst strength were expressed as a function of ZnO concentration and coating thickness. To increase the stability of the model fit, reduce collinearity, and facilitate the

comparison of coefficients, the independent variables were used in coded form. The factors were coded based on the central value and step change of each factor, such that the zero value corresponds to the center of the variation interval and positive and negative values indicate deviations from this center.

The quality and validity of the RSM models were assessed using a set of statistical criteria including coefficient of determination (R^2), adjusted coefficient of determination (Adj. R^2), lack-of-fit test, analysis of residual distribution for normality and homogeneity of variance, as well as prediction error indices such as RMSE and MAE. In addition, 3D response surface plots and contour plots were used for each response to visually display the simultaneous effects of factors and identify optimal regions in the design space.

2.10.4. Multi-response optimization

To determine the optimal process conditions, considering both antibacterial performance and mechanical properties, a multi-response optimization approach based on the desirability function was used. In this method, each response was converted into a desirability function in the range of 0 to 1, such that the maximization of the antibacterial index, tensile strength, and burst strength was simultaneously considered. The overall desirability of the system was defined as the geometric mean of the individual desirability, and the optimal conditions were selected as the combination of ZnO concentration and coating thickness with the highest overall desirability. In summary, the combined DOE–RSM approach used in this study allows for interpretable analysis of the effects of process factors and provides a reliable framework for the design and optimization of antibacterial paper coatings.

3. Results and Discussions

3.1. Structural analysis

Figure 2 shows the X-ray diffraction (XRD) patterns and crystallite size of the ZnO powder synthesized by the glycine–nitrate combustion method. As shown in the XRD patterns in Figure 2a, the successful completion of the combustion process and the formation of a pure ZnO phase (JCPDS No. 05-0664) can be confirmed, with no additional peaks corresponding to secondary phases, residual impurities, or intermediate compounds. In addition, the well-defined crystal structure and nanocrystalline nature of the ZnO particles are reflected in the high intensity of the main diffraction peaks along with their noticeable broadening, particularly at diffraction angles of approximately 31.7° and 36.2°. The crystallite size of the synthesized ZnO nanoparticles was estimated from the broadening of the main diffraction peaks using the Debye–Scherrer equation, and the corresponding results are illustrated in Fig. 2b. As shown in Figure 2b, based on the main diffraction peaks ((100), (002), (101), (102), and (110)), the calculated crystallite sizes range from 33 nm to 45 nm. Accordingly, the average crystallite size is 37 nm, while the maximum crystallite size reaches 45 nm. These results confirm the nanocrystalline nature of the synthesized ZnO particles. In combustion synthesis, the high rate of energy release and rapid cooling of the system prevent excessive grain growth and lead to the production of very small particles [9]. In biological applications, the small size of nanometer particles is an important advantage in improving antibacterial performance by increasing the specific active surface area and enhancing the interaction of particles with biological agents [8].

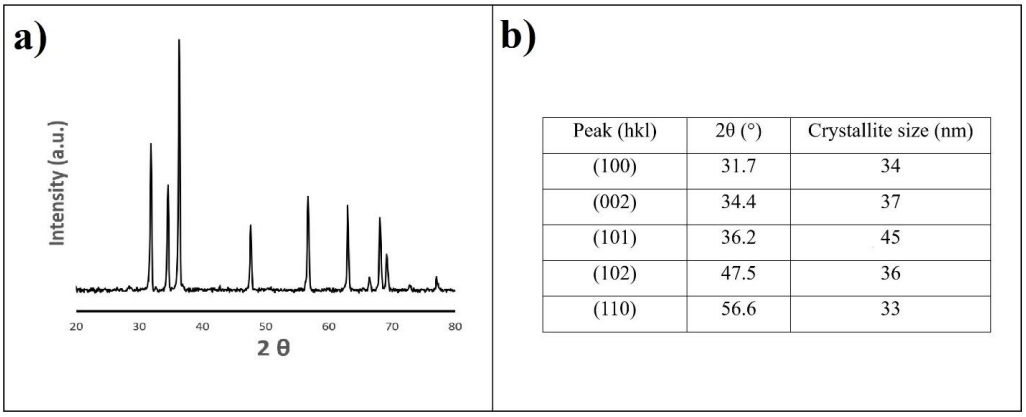

Peak (hkl)	2θ (°)	Crystallite size (nm)
(100)	31.7	34
(002)	34.4	37
(101)	36.2	45
(102)	47.5	36
(110)	56.6	33

Figure 2: XRD results of synthesized ZnO; a) XRD patterns, b) Crystallite size of synthesized ZnO nanoparticles calculated using the Debye–Scherrer equation

3.2. Morphology investigation

The morphology study of the synthesized ZnO nanoparticles was performed by scanning electron microscopy (SEM) and transmission electron microscopy (TEM) and results are presented in Figures 3a and 3b, respectively.

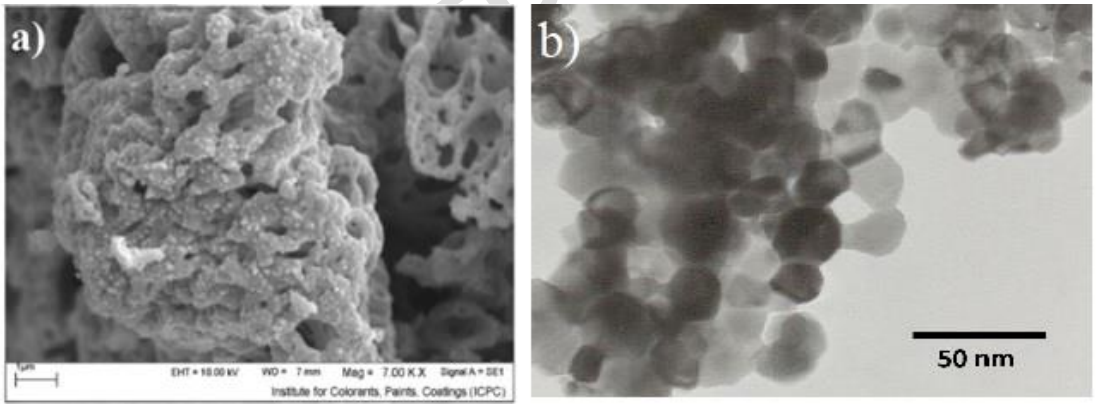

Figure 3: Scanning electron microscopy (a) and transmission electron microscopy (b) of t of as-synthesized ZnO

Figure 3a shows agglomerates with a porous structure, typical results of the combustion procedure. Rapid release of gases such as CO_2, N_2 and water vapor during the exothermic redox reaction leads to the creation of voids and the formation of a porous structure in the particles. Because the higher porosity and specific surface area This porosity is

considered as a good advantage in biological applications of zinc oxide particles. These allow for better dispersion and more uniform distribution of nanoparticles in the polymer matrix of the coating on the paper surface.

From Figure 3b, TEM image provides a clearer picture of the nanometer particle size and nearly spherical morphology of ZnO nanoparticles. The particle size observed in TEM images is in good agreement with the average crystallite size calculated from XRD results. Distinct particle boundaries and relative size uniformity indicate the formation of nanoparticles with proper crystal order. In antibacterial coating applications, the uniform morphology and nanometer size of ZnO particles make it an ideal choice, increasing the stability of the coating on the paper surface and more effective contact of nanoparticles with the surface and microorganisms.

The results of structural and morphological analyses suggest that the pure phase of ZnO and the desired size and shape can provide effective interaction of nanoparticles with microbial cells. Evaluation of the antibacterial performance of the synthesized ZnO nanoparticles seems to be an essential step. Therefore, minimum inhibitory concentration (MIC) and minimum bactericidal concentration (MBC) tests were subsequently investigated to determine the range of effective biological concentrations of nanoparticles and provide a scientific basis for their application in paper coatings.

3.3. Antibacterial activity of ZnO nanoparticles: MIC and MBC

Table 1 presents the results of the minimum inhibitory concentration (MIC) and minimum bactericidal concentration (MBC) tests of the synthesized ZnO nanoparticles against *Staphylococcus aureus* and *Escherichia coli* bacteria.

Table 1. MIC and MBC results of ZnO nanoparticles against **S. aureus** and **E. coli**

		ZnO concentration (mg/mL)									
Bacteria	**Test**	**0**	**0.1**	**0.5**	**1**	**1.5**	**2**	**2.5**	**3**	**3.5**	**4**
S. aureus	MIC	+	+	+	−	−	−	−	−	−	—
E. coli	MIC	+	+	+	+	−	−	−	−	−	—
S. aureus	MBC	+	+	+	+	−	−	−	−	−	—
E. coli	MBC	+	+	+	+	+	−	−	−	−	−

These results indicate that ZnO nanoparticles at relatively low concentrations are capable of inhibiting and killing *S. aureus* cells. In fact, the structure of the Gram-positive *S. aureus* cell wall lacks an outer lipopolysaccharide membrane, facilitating the penetration of nanoparticles or reactive oxygen species. It is observed that the antibacterial activity of ZnO nanoparticles is clearly concentration-dependent. For *S. aureus*, complete inhibition of bacterial growth was observed at a concentration of 1 mg/mL, which was determined as the MIC value, while the MBC value for this strain was 1.5 mg/mL. The closeness of the MIC and MBC values for both bacterial strains indicates the bactericidal nature of ZnO nanoparticles, such small increase in concentration above the inhibitory limit results in complete bacterial death. This behavior is consistent with the known mechanisms of antibacterial activity of ZnO, including the production of reactive oxygen species, damage to the cell membrane, and disruption of bacterial vital processes [18].

Higher concentrations of ZnO to inhibit the growth of *E. coli* than *S. aureus* is justified by the more complex structure of the cell wall of Gram-negative bacteria [19]. The presence of an outer lipopolysaccharide layer in *E. coli* may act as a protective barrier

and reduce the interaction of ZnO nanoparticles with bacterial cells [5, 16]. From Table 1 it is observed that the concentration of ZnO nanoparticles has a significant effect on the antibacterial activity against both bacterial strains studied. However, the MIC and MBC values obtained for *Staphylococcus aureus* were lower than the corresponding values for *Escherichia coli*, indicating a higher sensitivity of Gram-positive bacteria than Gram-negative bacteria.

The obtained MIC and MBC values provide a suitable scientific basis for determining the range of concentrations used in the design of experiments, so that, on the one hand, antibacterial efficacy is guaranteed and, on the other hand, excessive consumption of nanoparticles is prevented.

3.4. Antibacterial performance of ZnO–CMC coated paper as a function of ZnO concentration and coating thickness

The effect of ZnO nanoparticles concentration and coating thickness on the antibacterial activity of coated papers based on the antibacterial activity number (R) is shown in Figures 4a and 4b, respectively.

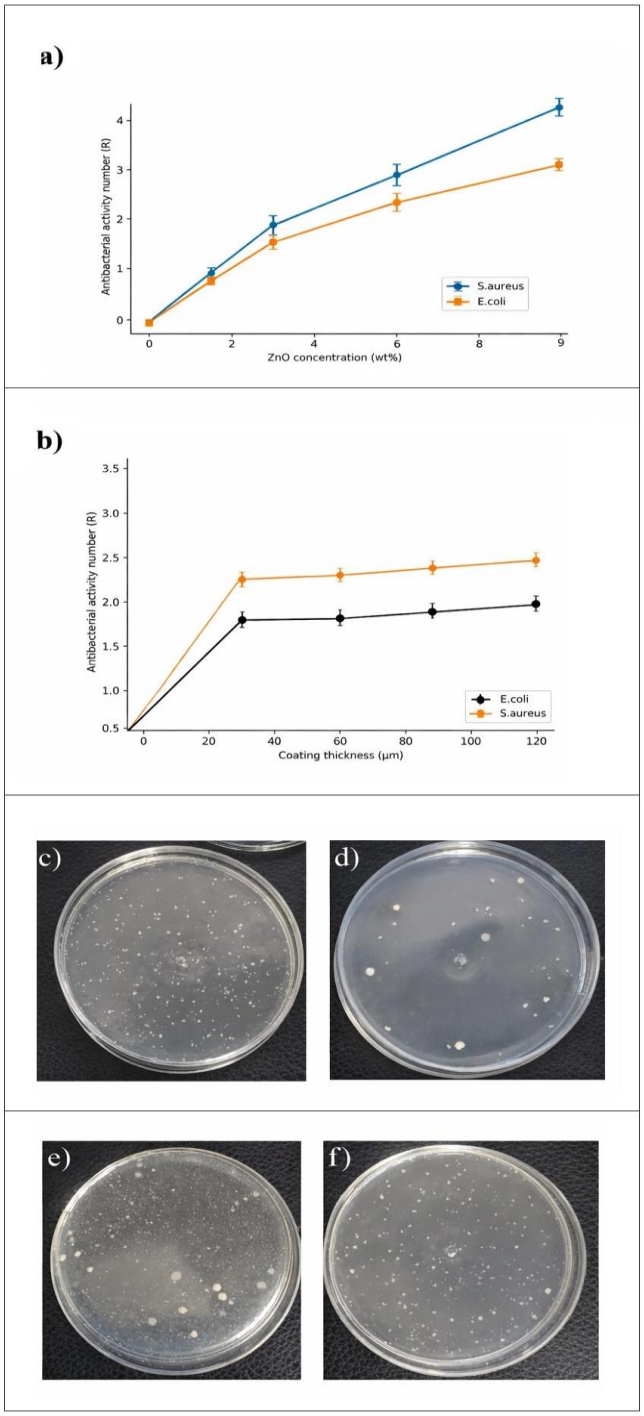

Figure 4. Antibacterial performance of ZnO–CMC coated paper (a) Antibacterial activity number (R) as a function of ZnO concentration; (b) Antibacterial activity number (R) as a function of coating thickness; (c) Agar plate image of *Staphylococcus aureus* for the control sample (uncoated paper, without ZnO); (d) Agar plate image of *Staphylococcus aureus* after contact with ZnO–CMC coated paper; (e) Agar plate image of *Escherichia coli* for the control sample (uncoated paper, without ZnO); (f) Agar plate image of *Escherichia coli* after contact with ZnO–CMC coated paper.

From Figure 4a concentration-dependent behavior of the system is observed with significant increase in the R value for both *Staphylococcus aureus* and *Escherichia coli*. In fact, an increase in the amount of ZnO nanoparticles leads to an increase in the number of antibacterial active centers on the coating surface, resulting in more effective contact with bacterial cells [20, 21]. Greater sensitivity of Gram-positive bacteria to the presence of ZnO nanoparticles is inferred from the higher R values for *S. aureus* compared to *E. coli*, consistent with the results of MIC and MBC tests.

While the structure of the cell wall of *S. aureus* is simpler compared to Gram-negative bacteria, it allows more effective interaction of nanoparticles or reactive oxygen species produced. In contrast, the lipopolysaccharide outer layer in *E. coli* acts as a permeability barrier against ZnO particles and reduces the intensity of the antibacterial effect to some extent. However, achieving significant R values at higher ZnO concentrations indicates that ZnO–CMC coatings have effective antibacterial performance even against Gram-negative bacteria [8, 21, 22].

Figure 4b presents the effect of coating thickness on antibacterial activity. It can be seen that as the thickness of the ZnO–CMC coating increases from 30 to 120 μm, a slight but detectable increase in the R value is observed for both bacterial strains. This behavior indicates that increasing the coating thickness likely leads to an increase in the amount of active nanoparticles per unit area and their continued contact with the bacterial environment. However, the effect of coating thickness is less important compared to the concentration of ZnO nanoparticles and the concentration of ZnO is recognized as the dominant factor in determining the antibacterial performance of the coatings.

These results show that while the antibacterial activity of paper coatings is affected by the

concentration of ZnO nanoparticles, the thickness of the coating plays a complementary and reinforcing role in improving this performance(23, 24). The observed concentration-dependent antibacterial response is in agreement with previously reported ZnO-based bio-coating systems, where higher nanoparticle content increases interfacial contact with bacterial cells and enhances oxidative stress mechanisms. The present findings align with this behavior and further confirm that ZnO concentration acts as the primary controlling parameter in the antibacterial performance of CMC-based coatings [5, 7, 22].

In addition to the quantitative evaluation based on the antibacterial activity number (R), representative photographs of bacterial growth on agar plates after contact with the coated paper samples are presented in Figure 4c–f. The control sample (without ZnO) shows dense bacterial colonies, whereas samples coated with ZnO–CMC exhibit a noticeable reduction in colony formation. The reduction in colony density becomes more pronounced with increasing ZnO concentration and coating thickness, visually confirming the concentration-dependent antibacterial behavior discussed above.

Figures 4c and 4d correspond to Staphylococcus aureus, while Figures 4e and 4f represent Escherichia coli. Consistent with the R-number results, a stronger inhibitory effect is observed against S. aureus, evidenced by fewer and smaller colonies compared to E. coli. These images support the quantitative antibacterial measurements and demonstrate the effective suppression of bacterial growth by ZnO–CMC coatings.

However, for practical applications, especially in the field of packaging and functional papers, achieving high antibacterial activity alone is not sufficient and maintaining or improving the mechanical properties of the paper is also of great importance. Therefore, it seems necessary to simultaneously investigate the effect of process parameters on

antibacterial performance and mechanical properties and identify the optimal conditions between these properties. In this regard, the effect of ZnO nanoparticles concentration and coating thickness on tensile strength and burst strength of coated papers is investigated and then design of experiments (DOE) and RSM modeling are used for multi-response analysis and optimization of the system.

3.5. Mechanical performance of ZnO–CMC coated paper

3.5.1. Tensile strength and elongation

The tensile and strain index at the breaking point (%) were measured as a function of the coating thickness and concentration of ZnO nanoparticles and results are shown in Figures 5 a-d.

a)

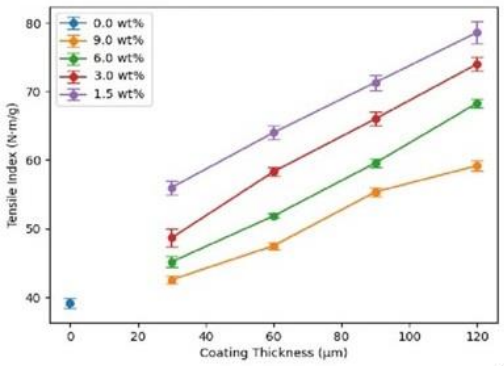

b)

ZnO (wt%)	Thickness (µm)	Tensile Index (N·m/g) (Mean ± SD)
0.0	0	39.17 ± 0.76
1.5	30	56.00 ± 1.00
1.5	60	64.00 ± 1.00
1.5	90	71.30 ± 1.13
1.5	120	78.60 ± 1.64
3.0	30	48.67 ± 1.26
3.0	60	58.30 ± 0.61
3.0	90	66.00 ± 1.00
3.0	120	74.00 ± 1.00
6.0	30	45.17 ± 0.76
6.0	60	51.85 ± 0.30
6.0	90	59.57 ± 0.59
6.0	120	68.30 ± 0.61
9.0	30	42.56 ± 0.51
9.0	60	47.50 ± 0.50
9.0	90	55.35 ± 0.65
9.0	120	59.17 ± 0.76

c)

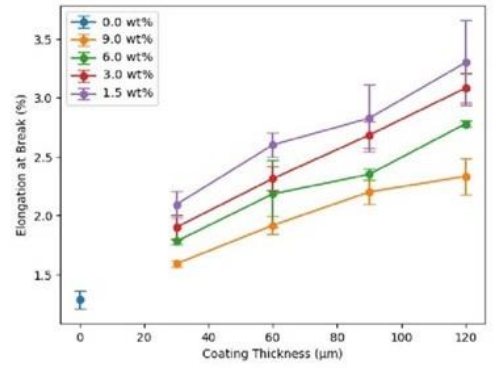

d)

ZnO (wt%)	Thickness (µm)	Elongation at Break (%) (Mean ± SD)
0.0	0	1.28 ± 0.08
1.5	30	2.09 ± 0.11
1.5	60	2.60 ± 0.10
1.5	90	2.83 ± 0.28
1.5	120	3.30 ± 0.36
3.0	30	1.90 ± 0.10
3.0	60	2.31 ± 0.10
3.0	90	2.68 ± 0.12
3.0	120	3.08 ± 0.13
6.0	30	1.78 ± 0.03
6.0	60	2.18 ± 0.28
6.0	90	2.35 ± 0.05
6.0	120	2.78 ± 0.03
9.0	30	1.59 ± 0.03
9.0	60	1.92 ± 0.08
9.0	90	2.20 ± 0.10
9.0	120	2.33 ± 0.15

Figure 5. Effect of ZnO nanoparticles concentration and coating thickness on mechanical properties of papers coated with ZnO–CMC: (a) Evolution of tensile index with coating thickness at different ZnO concentrations, (b) Tabulated values of tensile index (mean ± SD), (c) Evolution of elongation at break (%) with coating thickness at different ZnO concentrations, (d) Tabulated values of elongation at break (mean ± SD)

From Figure 5a, it can be seen that a significant increase in the tensile index is observed as the coating thickness increases from 30 to 120 microns. This incremental behavior can be attributed to the increase in the mass of the coating material on the paper surface, the more uniform coating layer, the filling of pores and surface irregularities, and ultimately the improvement of structural continuity in the surface area [25]. Moreover, at higher thicknesses, a more continuous and denser layer of CMC is created, which acts as a bridge between the fibers and helps transfer stress during force application.

In contrast, according to Figure 5a and 5b, a decreasing trend in tensile index was

observed at all thickness levels with increasing ZnO nanoparticle concentration**.** This behavior indicates that although ZnO nanoparticles play an effective role in providing antibacterial properties, they can mechanically weaken the cohesion of the CMC polymer network. In fact, incomplete dispersion of hard mineral nanoparticles in a polymer matrix can lead to the creation of concentrated stress points, from where failure can begin. The increase in particle agglomeration makes the stress transfer path discontinuous and consequently leads to a decrease in the tensile index [13, 25, 26].

Increasing the coating thickness shows a slight increasing effect on the elongation at break (%) value. Higher thicknesses, by creating a more uniform and continuous layer, make the stress distribution on the paper surface more homogeneous and consequently prevent the concentration of local stresses. However, the effect of thickness on the elongation at break is smaller and secondary to the effect of ZnO concentration (Figure 5c).

The strain behavior of the coatings at the breaking point (%) is shown in Figure 5d. The results demonstrate a decrease in elongation at break (%) with increasing ZnO nanoparticles concentration. This behavior indicates that the addition of excessive hard mineral nanoparticles restricts the mobility of CMC polymer chains. The creation of local discontinuities and stress concentration points in the polymer network makes the coating more brittle, leading to a reduction in fracture strain [25].

Therefore, increasing the ZnO concentration negatively affects both the tensile strength and elongation at break of the coating. This highlights a critical trade-off between mechanical properties and antibacterial performance in ZnO–CMC coatings. It emphasizes the importance of using design of experiments (DOE), RSM modeling, and

multi-response optimization to achieve an optimal combination of these conflicting responses.

3.5.2. Burst strength

The results of the burst strength of ZnO–CMC coated papers as a function of coating thickness and ZnO nanoparticle concentration are shown in Figure 6.

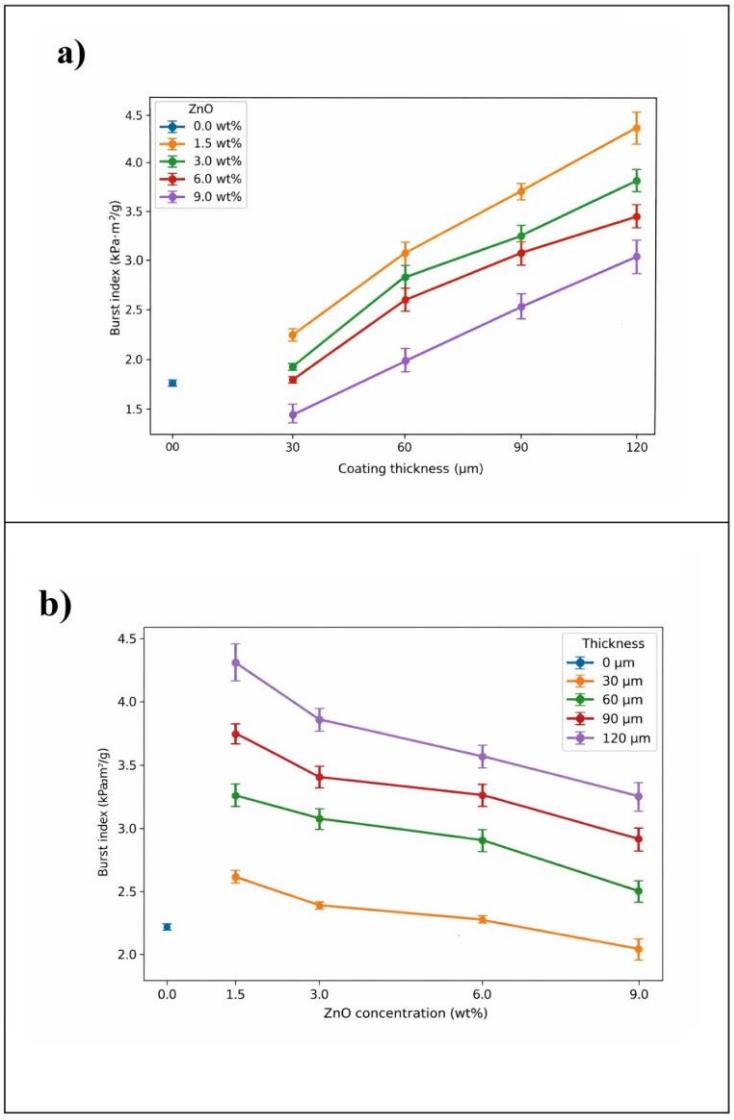

Figure 6. Effect of ZnO nanoparticles concentration and coating thickness on burst strength of papers coated with ZnO–CMC system: (a) Bursting index changes with coating thickness for different ZnO concentrations, (b) Bursting index changes with ZnO concentration for different coating thicknesses

From Figure 6a, increasing the coating thickness results in a significant increase in the burst index [25, 27]. This behavior can be attributed to the increase in the amount of coating material along with its more uniform and improved stress distribution on the paper surface [27, 28]. Since a more continuous and denser layer is formed at higher thicknesses, the bearing capacity of the coating in different directions increases and burst resistance improves [25, 29, 30]. However, according to Figure 6b, increasing the concentration of ZnO nanoparticles leads to a gradual decrease in the burst index at all thicknesses. This behavior, which was also observed in the tensile index, indicates a disruption in the continuity of the polymer network in the presence of mineral nanoparticles through the creation of stress concentration areas.

From Figures 5 and 6, it is concluded that the bursting behavior follows a similar trend to the tensile properties. While coating thickness plays a key role in improving both burst and tensile strengths by providing a denser structural network, increasing the concentration of ZnO nanoparticles disrupts this network and has a decreasing effect on these mechanical properties.

3.6. Brightness

Figure 7 shows the brightness of the paper at different coating thicknesses and different percentages of nano-ZnO. As the results of brightness measurement according to the TAPPI T 452 om-98 standard showed, the application of a coating containing carboxymethyl cellulose (CMC) and ZnO nanoparticles improved the optical properties of the paper. The uncoated paper had a brightness of 87% (TAPPI T 452), while after coating, an increase in brightness was observed.

As can be seen, increasing the percentage of nanoparticles from 1.5% to 6% by weight (w/w) led to a gradual improvement in brightness. This phenomenon can be attributed to the high refractive index of ZnO (about 2.0), which is significantly higher than the refractive index of cellulose fibers (about 1.53). The difference in refractive index between the mineral phase and the organic matrix increases the light-scattering coefficient in the coated layer and enhances diffuse reflectance at a wavelength of 457 nm (according to the TAPPI standard measurement). As a result, more light is reflected diffusely, leading to an increase in brightness. This increase continues with the addition of nano-ZnO up to a concentration of 6% by weight.

However, increasing the percentage of nanoparticles from 6% to 9% by weight did not yield a proportional increase in brightness, indicating a saturation effect. As observed in Figure 7, at lower and medium thicknesses (30 to 90 μm), the brightness of the 9 wt% samples is only marginally higher than that of the 6 wt% samples. More importantly, at the highest thickness (120 μm), the brightness value for the 9 wt% concentration actually falls below that of the 6 wt% sample. This behavior can be attributed to the coating layer reaching a saturation stage, where the probability of nanoparticle aggregation increases and the distance between particles decreases (optical crowding effect). Under such conditions, the independent scattering efficiency of each particle diminishes, reducing the effective refractive index contrast and leading to a plateau or slight decline in the brightness curve at high thicknesses.

On the other hand, as can be seen in Figure 7, the thickness of the coating also plays a decisive role in the optical behavior of the samples. At all ZnO concentrations, the brightness increased with increasing coating thickness from 30 to 120 μm. This can be

attributed to better coverage of the fiber network surface and a decrease in the light contribution of the underlying layer. Increasing the coating thickness increases the number of scattering surfaces per unit area and enhances the probability of diffuse reflection of light before it penetrates the fiber structure, which indicates that ZnO nanoparticles are capable of effectively modifying the optical properties even in thin layers.

Also, if we examine the effect of nanoparticle concentration and coating thickness simultaneously in this study, the results show that the relationship between these two parameters is not completely linear. At low nanoparticle concentrations, increasing the thickness has a milder effect, while in the middle range (about 3 to 6 wt.%) the synergistic effect between the nanoparticle content and coating thickness is more noticeable. At 9 wt.%, a further increase in thickness leads to a more limited improvement in brightness, indicating that the system has reached the scattering saturation region.

Accordingly, it seems that 6 wt.% ZnO content combined with higher coating thicknesses provides the best balance between nanoparticle consumption and brightness improvement. Overall, the brightness improvement in this system is mainly due to the increase in diffuse light reflectance resulting from the difference in refractive index between ZnO nanoparticles and the cellulose matrix. Therefore, controlling the uniformity of nanoparticle distribution and preventing their aggregation at high loadings plays a key role in optimizing the optical performance of the coating. The results indicate that the targeted use of ZnO nanoparticles in CMC-based coating systems can be an effective way to improve the optical properties of paper without the need for chemical

bleaching additives. Similar improvements in brightness have been reported in nanoparticle-filled coating systems, where enhanced refractive index contrast and uniform nanoparticle dispersion contribute to increased diffuse light scattering and optical performance which is in line with the results of this study [31, 32]. Improved optical performance in nanoparticle-modified coatings has been attributed to enhanced light scattering and reflectance due to refractive index contrast between inorganic particles and the paper matrix. For instance, embedded TiO_2 nanoparticles have been shown to significantly increase coating reflectance due to enhanced radiative properties. Moreover, nano-pigments influence brightness and diffuse reflectance in coated papers, which supports the role of particle size and dispersion in optical behavior. In the context of paper brightness measurement, enhanced diffuse light scattering contributes directly to brightness values [33, 34].

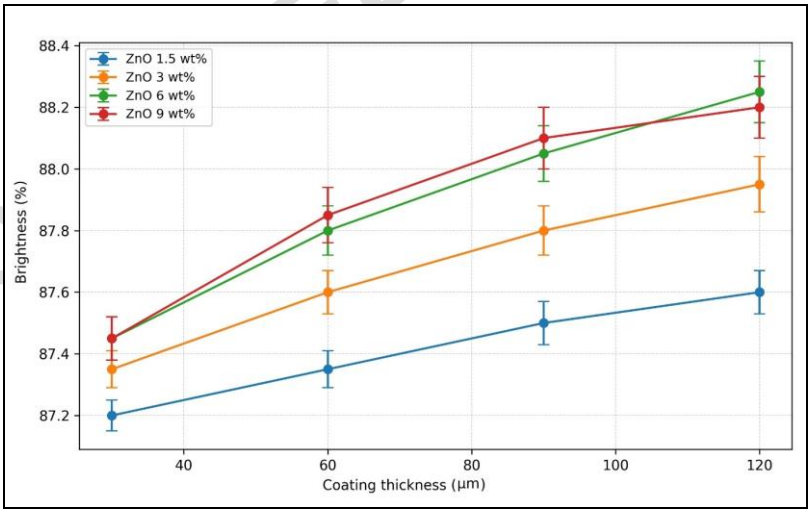

Figure 7. Brightness of papers with different coating thicknesses and different weight percentages of ZnO nanoparticles

3.6. DOE and RSM analysis

3.6.1. Statistical analysis based on DOE (Two-way ANOVA)

Based on a full factorial experimental design with two factors including ZnO nanoparticles concentration (A) and coating thickness (B), two-way analysis of variance (ANOVA) was performed to investigate the main effects and interaction of these factors on the antibacterial performance and mechanical properties of papers coated with the ZnO–CMC system. The responses examined included antibacterial activity number (R), tensile index, strain at break (Break %) and burst index. The results are given in Table 2.

Table 2. Two-way ANOVA summary for antibacterial and mechanical responses of ZnO–CMC coated paper

Response	Factor	Statistical significance
Antibacterial activity (R)	ZnO concentration (A)	Significant ($p < 0.001$)
Antibacterial activity (R)	Coating thickness (B)	Not significant ($p > 0.05$)
Antibacterial activity (R)	A × B	Significant ($p < 0.001$)
Tensile index	ZnO concentration (A)	Significant ($p < 0.001$)
Tensile index	Coating thickness (B)	Significant ($p < 0.001$)
Tensile index	A × B	Significant ($p < 0.0۵$)
Elongation at break	ZnO concentration (A)	Significant ($p < 0.0۰۱$)
Elongation at break	Coating thickness (B)	Significant ($p < 0.001$)
Elongation at break	A × B	Significant ($p < 0.0۵$)
Burst index	ZnO concentration (A)	Significant ($p < 0.001$)
Burst index	Coating thickness (B)	Significant ($p < 0.001$)
Burst index	A × B	Significant ($p < 0.0۵$)

The ANOVA results showed that the behavior of this system is generally nonlinear and strongly dependent on the interaction of factors, such that the interaction effect of ZnO concentration and coating thickness (A×B) was found to be statistically significant for all responses. Such behavior clearly justifies the necessity of using DOE-based approaches and response surface modeling (RSM). The results show that increasing the ZnO concentration led to a significant increase in the R number, indicating the important effect of the concentration of ZnO nanoparticles (A) in determining the antibacterial performance of the coating. However, this same factor has an adverse effect on mechanical properties, and with increasing ZnO concentration, we see a decrease in tensile index and burst index.

Although, the coating thickness did not have a decisive effect on the R number, it is able to improve the stability of the antibacterial performance in interaction with the ZnO concentration. The ANOVA results showed that the A × B interaction effect was highly significant for all four responses (R, tensile index, Break % and burst index). This result suggests that increasing the thickness can partially moderate the negative effects of high ZnO concentration on mechanical strength, while still maintaining a high level of antibacterial activity. In conclusion, interpreting the results only based on the main factors can be misleading, and simultaneous examination of the factors can provide a true picture of the system's behavior. The ANOVA results statistically demonstrate that the design of ZnO–CMC coatings require a conscious trade-off between antibacterial performance and mechanical integrity. These findings quantitatively and qualitatively support the need to use RSM modeling and multi-response optimization to achieve an optimal combination of high R-number and acceptable mechanical properties [35].

From a process compatibility perspective, the selection of ZnO concentration and coating thickness as independent variables is strongly supported by the statistical results of the DOE analysis. Although the main effects of individual factors were always statistically significant for mechanical properties, the interaction term (A × B) was highly significant for all responses, including antibacterial activity, tensile index, elongation at break, and burst index.

This indicates that the behavior of the ZnO–CMC system is governed primarily by the combined effect of nanoparticle loading and structural thickness rather than by isolated factor contributions. Increasing ZnO concentration significantly enhances antibacterial performance; however, excessive nanoparticle incorporation may reduce mechanical

integrity. Increasing coating thickness, on the other hand, reinforces the matrix and partially compensates for this weakening effect.

Therefore, these two factors represent the most critical and industrially adjustable variables that determine the compatibility between biological functionality and mechanical stability. The statistical evidence of strong interaction justifies their simultaneous investigation through full factorial DOE and RSM modeling.

3.6.2. Response Surface Modeling (RSM) and Simultaneous analysis of antibacterial and mechanical responses of ZnO–CMC system

In order to quantitatively characterize the behavior of the ZnO–CMC system and investigate the simultaneous effect of ZnO nanoparticle concentration and coating thickness on the functional properties, the experimental data obtained from a full factorial experimental design were analyzed using the response surface modeling (RSM) method. In this regard, two independent factors including ZnO concentration (A, (wt%)) and coating thickness (B, (µm)) were considered and for each of the responses, a quadratic model including linear effects, quadratic terms and a factor interaction term was fitted. The general form of the model used is expressed as equation 4:

$$Y = \beta_0 + \beta_1 A + \beta_2 B + \beta_{12} AB + \beta_{11} A^2 + \beta_{22} B^2 \quad (4)$$

Where Y represents one of the responses including antibacterial activity number (R) for each bacterial strain, tensile index, strain at break point and burst index. The coefficients of the models were estimated using the least squares method based on raw data and their statistical significance was evaluated through the p-value test.

The results of the model fitting, whose coefficients are presented in detail in Table 3,

show that the quadratic models are able to explain a major part of the variations in the mechanical responses of the system. The high values of the adjusted coefficients of determination (Adj. R^2) for the tensile index (0.948), the fracture strain (0.921) and the burst index (0.965) indicate the statistical adequacy of the models and their high ability to predict the behavior of the system within the design range. Also, the significant linear coefficients of the coating thickness in all mechanical responses confirm the dominant role of this factor in determining the mechanical performance of the coating, while the negative coefficients of ZnO concentration for the tensile and burst indices indicate the weakening effect of nanoparticles in some conditions.

Table 3. RSM quadratic model coefficients and statistical significance for mechanical responses (A: ZnO concentration (wt%), B: coating thickness)

Response	Term	Coefficient	p-value	R^2	Adj. R^2
Tensile index (N·m/g)	β_0	39.2347	<0.001	**0.959**	**0.94۸**
	A	−2.2701	<0.001		
	B	+0.1710	<0.001		
	A^2	+0.1001	0.022		
	B^2	+0.000141	0.565		
	AB	+0.00656	0.012		
Break (%)	β_0	1.3747	<0.001	**0.925**	**0.917**
	A	-0.۰۷۳۶	0.۰۰۰۱		
	B	+0.0۲۲۸28	<0.001		
	A^2	−0.0۰669	0.0515		
	B^2	−0.000004	0.027		
	AB	+0.000976	۰/۰۳		
Burst index (kPa·m²/g)	β_0	2.1084	<0.001	**0.982**	**0.9۶۵**
	A	−0.13231	<0.001		
	B	+0.025812	<0.001		
	A^2	+0.004616	0.124		
	B^2	−0.000048	0.00664		
	AB	−0.000400	0.0257		

To interpret the behavioral models, the three-dimensional response surfaces and corresponding contour plots for all responses are presented in Figure 8. As can be seen in panels (a) and (b), the antibacterial activity number (R) against Staphylococcus aureus

and Escherichia coli shows a uniform but nonlinear increasing trend with increasing ZnO concentration and coating thickness. The dominant slope of the response surfaces along the ZnO concentration axis indicates the determining role of the amount of nanoparticles in increasing the antibacterial performance, while the coating thickness has a reinforcing and complementary effect. However, the R values against E. coli are lower than the corresponding values for S. aureus over the entire design range, which can be attributed to the lower sensitivity of Gram-negative bacteria to ZnO nanoparticles.

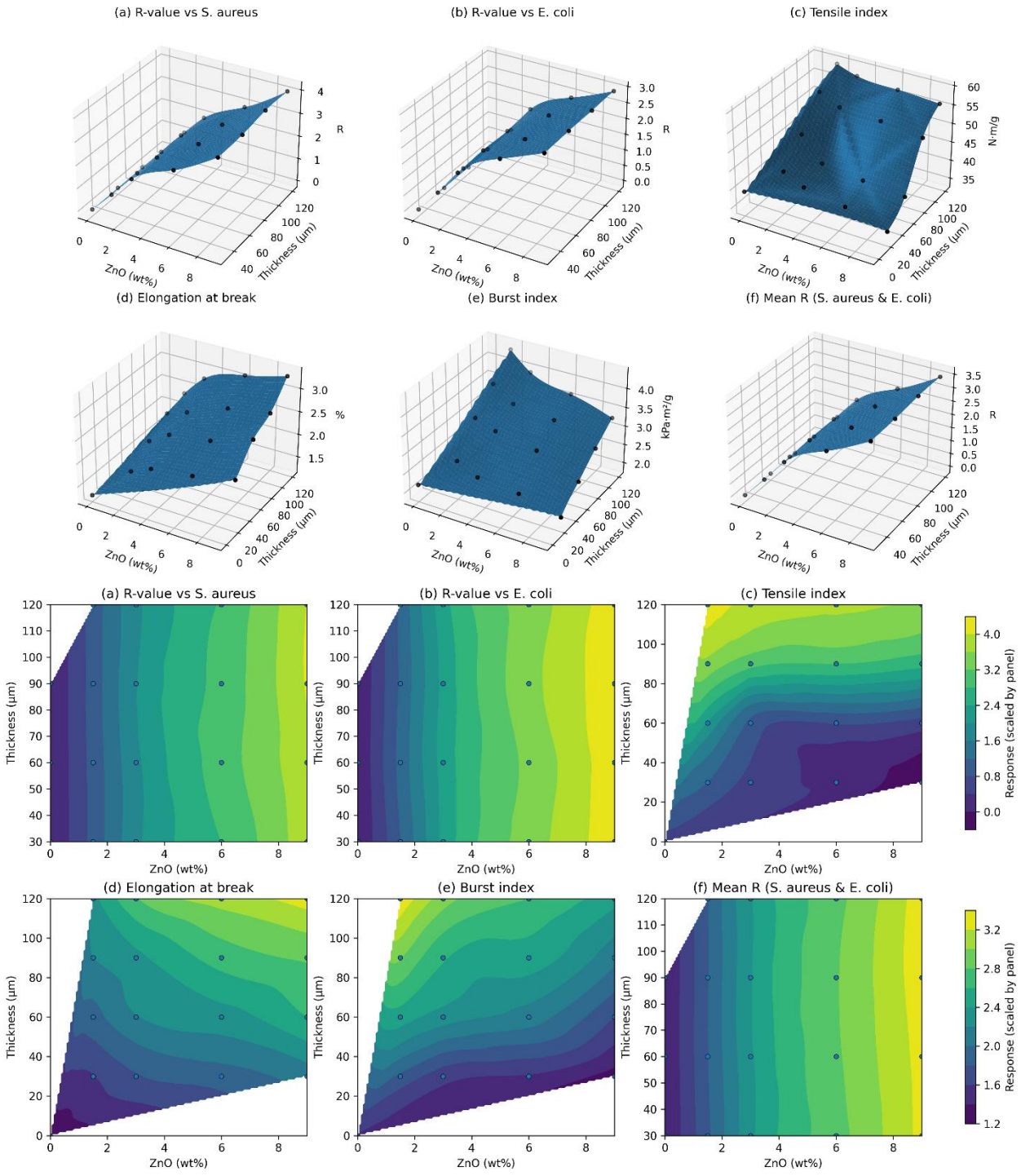

Figure 8. Response surface plots (a–f) and contour plots (bottom row) obtained from response surface modeling (RSM) based on a full factorial experimental design for the ZnO–CMC system in the design space including ZnO nanoparticles concentration (wt%) and coating thickness (μm). Panels (a) and (b) show the changes in antibacterial activity number (R) against Staphylococcus aureus and Escherichia coli, respectively, while panel (f) presents the average R value for both strains to summarize the antibacterial performance. Panels (c), (d), and (e) show the tensile index, strain at break (Break %), and burst index of the coated papers, respectively.

The mechanical behavior of the coatings is simultaneously affected by both factors. According to panel (c), the tensile index is strongly dependent on the coating thickness, increasing the thickness leads to a significant increase in tensile strength. This could be attributed to the formation of a more continuous and denser layer of CMC and the strengthening of the role of mechanical bridges between the fibers. In contrast, increasing ZnO concentration in most regions of the design space is associated with a decrease in the tensile index, due to increased microstructural heterogeneity, stress concentration, and the possibility of nanoparticles agglomeration in the polymer matrix. Table 3 demonstrates a significant presence of the AB interaction term, indicating negative effect of ZnO at higher thicknesses.

According to panel (d), the elongation at break shows a complex behavior. While it consistently increases with coating thickness, indicating improved ductility, the addition of ZnO tends to reduce this property. On the other hand, the burst index (panel (e)) shows the sensitivity to coating thickness, and increasing the thickness leads to a significant improvement in burst strength, while increasing the ZnO concentration in some regions of the design space is associated with a decrease in this index. The curvature of the response surfaces and the equivalent lines indicate the nonlinear nature of this response and its dependence on the interaction of the coating microstructure and the distribution of nanoparticles.

To summarize the antibacterial performance, panel (f) displays the average R-number for both bacterial strains as an aggregate response. This plot clearly identifies the region of the design space where simultaneous increases in ZnO concentration and coating thickness lead to maximum antibacterial activity.

The good fit of the experimental points with the predicted RSM surfaces in Fig. 8 and the significance of the coefficients presented in Table 3 indicate that the employed quadratic models are able to accurately describe the behavior of the ZnO–CMC system. It should be noted that in Fig. 8, the black dots on the plots represent the experimental values obtained from DOE, and the solid surfaces and equivalent lines represent the predictions of the quadratic RSM model. These plots show the main and interaction effects of ZnO concentration and coating thickness on the antibacterial and mechanical properties and identify the optimal performance regions in the design space. Therefore, the close agreement between experimental data points and predicted RSM surfaces confirms the adequacy and robustness of the fitted quadratic models. Moreover, the low standard deviation among experimental replicates further supports the internal consistency, reproducibility, and reliability of the dataset used for RSM modeling.

3.6.3. Multi-responses optimization based on the desirability function (Desirability Optimization)

To determine the optimal process conditions considering simultaneously the antibacterial performance and mechanical properties of ZnO–CMC coated papers, multi-responses optimization was performed. The outputs of the quadratic RSM models were used in the Desirability Function approach. This approach allows the integration of multiple heterogeneous responses into a single criterion and leads to the selection of conditions in which a reasonable compromise between biological efficiency and mechanical integrity is achieved.

In this method, each response is transformed into a dimensionless utility function d_i in the

range of zero to one, such that a value of zero indicates the most undesirable situation and a value of one indicates the best performance of that response. In this study, the optimization objectives included maximizing the antibacterial activity number (R) for both *Staphylococcus aureus* and *Escherichia coli* strains, maximizing the tensile index and burst index; while the strain at break (Break %) was defined as a target within an acceptable range (in-range) to maintain the flexibility of the coating and prevent brittleness or impractical behaviors. The overall system utility (D) was defined as the geometric mean of individual of utilities, which is expressed as equation (5):

$$D = (d_1 \times d_2 \times d_3 \times d_4 \times d_5)^{1/5} \quad (5)$$

Where d_1 to d_5 are the desirability values of the antibacterial activity against *S. aureus*, antibacterial activity against *E. coli*, tensile index, burst index, and elongation at break, respectively. Using the geometric mean causes the poor performance of any response to significantly reduce the overall desirability of the system, thus preventing the selection of conditions with unbalanced and one-dimensional performance.

Based on the optimization of the overall utility function, the optimal region in the design space was identified in the range of intermediate ZnO concentrations and relatively high thicknesses. The results showed that the optimal point is located at a ZnO concentration of 7.55 wt% and a coating thickness of 120 µm. Under these conditions, the antibacterial activity number for both bacterial strains shows high values, while the tensile and bursting indices are maintained at acceptable and desirable levels and the fracture strain value is also within the defined target range. The predicted values of the responses at this optimal point are presented in detail in Table 4.

Table 4. Optimal conditions and predicted values (RSM–Desirability)

Parameters	Optimal values
ZnO (wt%)	**7.55**
Thickness (µm)	**120**
R (S. aureus)	3.57
R (E. coli)	2.74
Tensile index (N·m/g)	56.30
Burst index (kPa·m²/g)	3.42
Elongation at Break (%)	3.20
Overall desirability (D)	0.823

Analysis of the optimization results shows that excessive increase in ZnO concentration, although leading to further improvement in antibacterial performance, is accompanied by a decrease in mechanical properties and ultimately reduces the overall desirability of the system. Moreover, the selection of intermediate ZnO concentrations along with higher coating thicknesses strikes a good balance between these two aspects. From a physical perspective, higher coating thickness, partially compensates for the negative effects caused by the presence of ZnO nanoparticles. This also enables simultaneous achievement of high antibacterial activity and stable mechanical properties.

Results demonstrate that the combined DOE–RSM approach is an effective tool for the systematic design of ZnO–CMC coatings, allowing the selection of optimal process conditions without relying on experimental trial and error. This framework provides a quantitative, defensible, and generalizable strategy for the development of multifunctional antibacterial coatings for paper and packaging applications.

4. Conclusions

In this study, a multi-functional antibacterial paper coating was successfully developed using a green, energy-efficient glycine-nitrate combustion synthesis of ZnO nanoparticles dispersed in a carboxymethyl cellulose (CMC) matrix. Structural characterizations

confirmed the formation of pure ZnO nanoparticles with an average crystallite size of 37 nm. The synthesized nanoparticles exhibited strong intrinsic antibacterial activity. The Minimum Inhibitory Concentration (MIC) and Minimum Bactericidal Concentration (MBC) values were 1 mg/mL and 1.5 mg/mL against *S. aureus*, and 1.5 mg/mL and 2 mg/mL against *E. coli*, respectively. Applying the ZnO-CMC coating on the paper substrate not only provided structural integrity but also slightly improved the optical properties. To resolve the inherent trade-off between the antibacterial efficiency of nanoparticles and the mechanical stability of the paper, Response Surface Methodology (RSM) based on a full factorial design was employed. The statistical analysis revealed a highly significant interaction between ZnO concentration and coating thickness across all evaluated responses. Multi-response desirability optimization identified the optimal formulation at a ZnO concentration of 7.55 wt.% and a coating thickness of 120 µm (overall desirability = 0.823). Under these optimal conditions, the coated paper demonstrated excellent antibacterial performance, achieving R-values of 3.57 against *S. aureus* and 2.74 against *E. coli* Simultaneously, the mechanical integrity of the paper was well-preserved, yielding a tensile index of 56.30 N·m/g, a burst index of 3.42 kPa·m2/g, and an enhanced elongation at break of 3.20% (compared to 1.28% for the base paper). Ultimately, this study provides a quantitatively validated and environmentally compatible framework for designing scalable, active packaging materials with a statistically optimized balance of biological and mechanical properties.

5. References

1. Cruz RMS, Rico BPM, Vieira MC. 9 - Food packaging and migration. In: Galanakis CM, editor. Food Quality and Shelf Life: Academic Press; 2019. p. 281-301. https://doi.org/10.1016/B978-0-12-817190-5.00009-4

2. Mortazavi Moghadam FA, Khoshkalampour A, Mortazavi Moghadam FA, PourvatanDoust S, Naeijian F, Ghorbani M. Preparation and physicochemical evaluation of casein/basil seed gum film integrated with guar gum/gelatin based nanogel containing lemon peel essential oil for active food packaging application. Inter J Biol Macromol. 2023; 224:786-96. https://doi.org/10.1016/j.ijbiomac.2022.10.166

3. Rao MMV, Mohammad N, Banerjee S, Khanna PK. Synthesis and food packaging application of silver nano-particles: A review. Hybrid Adv. 2024; 6:100230. https://doi.org/10.1016/j.hybadv.2024.100230

4. Mortazavi Moghadam Fs, Mortazavi Moghadam FA. Kombucha fungus bio-coating for improving mechanical and antibacterial properties of cellulose composites. Mater Today Commun. 2024; 40:109609. https://doi.org/10.1016/j.mtcomm.2024.109609

5. Mendes CR, Dilarri G, Forsan CF, Sapata VMR, Lopes PRM, de Moraes PB, et al. Antibacterial action and target mechanisms of zinc oxide nanoparticles against bacterial pathogens. Sci Rep. 2022; 12(1):2658. https://doi.org/10.1038/s41598-022-06657-y

6. Mortazavi Moghadam FA, Resalati H, Rasouli S, Asadpour G. New method of producing nanominerals from office paper waste and investigating their microstructural properties. Biomass Conversion Biorefinery. 2022. https://doi.org/10.1007/s13399-022-02782-w

7. Onyszko M, Markowska-Szczupak A, Rakoczy R, Paszkiewicz O, Janusz J, Gorgon-Kuza A, et al. The cellulose fibers functionalized with star-like zinc oxide nanoparticles with boosted antibacterial performance for hygienic products. Sci Reports. 2022;12(1):1321. https://doi.org/10.1038/s41598-022-05458-7

8. Mohammed AM, Mohammed M, Oleiwi JK, Ihmedee FH, Adam T, Betar BO, et al. Comprehensive review on zinc oxide nanoparticle production and the associated antibacterial mechanisms and therapeutic potential. Nano Trends. 2025; 11:100145. https://doi.org/10.1016/j.nwnano.2025.100145

9. Vitasovic T, Caniglia G, Eghtesadi N, Ceccato M, Jesen E, Gosewinkel U, et al. Antibacterial Action of Zn^{2+} Ions Driven by the In Vivo Formed ZnO Nanoparticles. ACS Appl Mater Inter. 2024; 16. https://doi.org/10.1021/acsami.4c04682

10. El-Habib I, Maatouk H, Lemarchand A, Dine S, Roynette A, Mielcarek C, et al. Antibacterial Size Effect of ZnO Nanoparticles and Their Role as Additives in Emulsion Waterborne Paint. J Function Biomater. 2024; 15(7):195. https://doi.org/10.3390/jfb15070195

11. Ursu D, Casut C, Miclau M. Elaboration of new materials using hydrothermal methods. Materials. 2022; 15(21):7792. https://doi.org/10.3390/ma15217792

12. Chang BP, Md Akil H, Nasir R, Bandara CC, Rajapakse S. The effect of ZnO nanoparticles on the mechanical, tribological and antibacterial properties of ultra-high molecular weight polyethylene. J Reinf Plastic Composit. 2013; 33:674-86. https://doi.org/10.1177/0731684413509426

13. Kalliampakou KI, Athanasopoulou E, Spanou A, Flemetakis E, Tsironi T. In vitro cytotoxicity evaluation of a CMC-SA edible packaging film for migration and safety assessment. Sci Rep. 2025; 15(1):13304. https://doi.org/10.1038/s41598-025-98163-0

14. Gudkov S, Burmistrov D, Serov D, Rebezov M, Семенова A, Lisitsyn A. A Mini Review of Antibacterial Properties of ZnO Nanoparticles. Frontiers Phy. 2021; 9:641481. https://doi.org/10.3389/fphy.2021.641481

15. Sirelkhatim A, Mahmud S, Seeni A, Kaus NHM, Ann LC, Bakhori SKM, et al. Review on Zinc Oxide Nanoparticles: Antibacterial Activity and Toxicity Mechanism. Nano-micro Let. 2015; 7(3):219-42. https://doi.org/10.1007/s40820-015-0040-x

16. Mortazavi Moghadam FS, Rasouli S, Mortazavi Moghadam FA. In Vivo Study and Cytotoxicity of Migrated Silver Nanoparticles (AgNPs) from Cellulose/LDPE/AgNP Nanocomposite in Highly Perishable Food (Fish Fillet) Packaging. ACS Food Sci Technol. 2025. https://doi.org/10.1021/acsfoodscitech.4c00850

17. Wang Y, Coppel Y, Lepetit C, Marty JD, Mingotaud C, Kahn ML. Anisotropic growth of ZnO nanoparticles driven by the structure of amine surfactants: the role of surface dynamics in nanocrystal growth. Nanoscale Adv. 2021; 3(21):6088-99. https://doi.org/10.1039/d1na00566a

18. Kumar PM, Babujanarthanam R, Selvi RT, Ganesamoorthy R, Sudan SJJ, Kasthuri K, et al. Spherical-shaped ZnO nanoparticles and their diverse surface morphological applications in various biological applications against ROS. Appl Phys A. 2025; 131(5):379. https://doi.org/10.1007/s00339-025-08504-z

19. González SCE, Bolaina-Lorenzo E, Pérez-Trujillo JJ, Puente-Urbina BA, Rodríguez-Fernández O, Fonseca-García A, et al. Antibacterial and anticancer activity of

ZnO with different morphologies: a comparative study. 3 Biotech. 2021; 11(2):68. https://doi.org/10.1007/s13205-020-02611-9

20. Ouf MSM, Duab MEA, Abdel-Meguid DI, El-Sharouny EE, Soliman NA. Biogenic Zinc nanoparticles: green approach to synthesis, characterization, and antimicrobial applications. Microbial cell factories. 2025; 24(1):168. https://doi.org/10.1186/s12934-025-02788-9

21. Babayevska N, Przysiecka Ł, Iatsunskyi I, Nowaczyk G, Jarek M, Janiszewska E, et al. ZnO size and shape effect on antibacterial activity and cytotoxicity profile. Sci Rep. 2022; 12(1):8148. https://doi.org/10.1038/s41598-022-12134-3

22. Jayasuriya AC, Aryaei A, Jayatissa AH. ZnO nanoparticles induced effects on nanomechanical behavior and cell viability of chitosan films. Materials science & engineering C, Mater Biol Appl. 2013; 33(7):3688-96. https://doi.org/10.1016/j.msec.2013.04.057

23. Tamulevičienė A, Mardosaitė R, Ilickas M, Abakevičienė B, Tamulevičius T, Meškinis Š, et al. Highly-hydrophobic, transparent, and durable coatings based on ZnO tetrapods with diamond-like carbon nanocomposite. Surf Coat Technol. 2023; 470:129863. https://doi.org/10.1016/j.surfcoat.2023.129863

24. Mortazavi Moghadam FA, Resalati H, Rasouli S, Asadpour G. Fabrication of high mechanical properties papers coated with CMC-based nanocomposites containing nanominerals synthesized from paper waste. Cellulose. 2021; 28(17):11153-64. https://doi.org/10.1007/s10570-021-04241-7

25. He C, Hu Y, Yin L, Tang C, Yin C. Effects of particle size and surface charge on cellular uptake and biodistribution of polymeric nanoparticles. Biomater. 2010; 31(13):3657-66. https://doi.org/10.1016/j.biomaterials.2010.01.065

26. Mortazavi Moghadam Fs, Rasouli S. Recycling kaolin from paper waste and assessment of its application for paper coating. Mater Today Commun. 2024; 39:109142. https://doi.org/10.1016/j.mtcomm.2024.109142

27. Oztemur J, Ozdemir S, Sezgin H, Yalcin Enis I. Investigation of the effects of polymer type and fiber orientation on burst strength of the tTubular scaffolds by multilevel full factorial design. 2024. p. 66-71. https://doi.org/10.2478/9788367405355-011

28. Demirci S, Sutekin SD, Sahiner N. Polymeric composites based on carboxymethyl cellulose cryogel and conductive polymers: synthesis and characterization. J Comp Sci. 2020 ;4(2). https://doi.org/10.3390/jcs4020033

29. Mortazavi F, Resalati H, Rasouli S, Asadpour G. Investigation of industrial paper coating with recycled kaolin. J Color Sci Technol. 2021; 15(2):117-29. https://doi.org/20.1001.1.17358779.1400.15.2.4.1

30. Prasad V, Shaikh AJ, Kathe AA, Bisoyi DK, Verma AK, Vigneshwaran N. Functional behaviour of paper coated with zinc oxide–soluble starch nanocomposites. J Mater Proce Technol. 2010; 210(14):1962-7. https://doi.org/10.1016/j.jmatprotec.2010.07.009

31. Chokboribal J, Amornkitbamrung L, Somchit W, Suchaiya V, Khamweera P, Pankaew P. Effects of ZnO/trimethylsilyl cellulose nano-composite coating on anti-UV

and anti-fungal properties of papers. Sci Reports. 2023; 13(1):20714. https://doi.org/10.1038/s41598-023-45853-2

32. Dias C, Veloso RC, Maia J, Ramos NMM, Ventura J. Oversight of radiative properties of coatings pigmented with TiO_2 nanoparticles. Energy Buildings. 2022; 271:112296. https://doi.org/10.1016/j.enbuild.2022.112296

33. Gong R, Fleming PD, Sönmez S. Application of nano pigments in inkjet paper coating. International Conference on Digital Printing Technologies. 2010; 26:507-11. https://doi.org/10.2352/ISSN.2169-4451.2010.26.1.art00035_2

34. Vukmanović S, Vitas J, Ranitović A, Cvetković D, Tomić A, Malbaša R. Certain production variables and antimicrobial activity of novel winery effluent based kombucha. LWT. 2022;154:112726. https://doi.org/10.1016/j.lwt.2021.112726